Journal of Biomedical Optics

SPIEDigitalLibrary.org/jbo

# Smart surgical tool

Huan Huang
Lih-Mei Yang
Shuang Bai
Jian Liu

SPIE

Journal of Biomedical Optics 20(2), 028001 (February 2015)

# Smart surgical tool

**Huan Huang,[a,*] Lih-Mei Yang,[b] Shuang Bai,[a] and Jian Liu[a]**
[a]PolarOnyx, Inc., 2526 Qume Drive, Suite 17 & 18, San Jose, California 95131, United States
[b]PolarOnyx Laser, Inc., 2526 Qume Drive, Suite 18, San Jose, California 95131, United States

**Abstract.** A laser-induced breakdown spectroscopy (LIBS) guided smart surgical tool using a femtosecond fiber laser is developed. This system provides real-time material identification by processing and analyzing the peak intensity and ratio of atomic emissions of LIBS signals. Algorithms to identify emissions of different tissues and metals are developed and implemented into the real-time control system. This system provides a powerful smart surgical tool for precise robotic microsurgery applications with real-time feedback and control.  [DOI: 10.1117/1.JBO.20.2.028001]

Keywords: surgical tool; femtosecond lasers; fiber laser; laser-induced breakdown spectroscopy.

Paper 140547PRR received Aug. 28, 2014; accepted for publication Jan. 8, 2015; published online Feb. 3, 2015.

## 1 Introduction

Ultrashort pulsed lasers (femtosecond or picosecond pulse duration/width) have increasingly been gaining popularity and are known to be ideal tools for the high quality microstructuring of different materials. The high peak intensity results in fundamentally different laser material interaction mechanisms—nonlinear absorption through photoionization and avalanche ionization. The ultrashort pulsed laser has unprecedented advantages over long pulsed lasers in that it generates photoionization and plasma formation in less than a picosecond. This process is much shorter than the thermal diffusion time (> ns). Therefore, the thermal damage to surrounding materials is minimal. In contrast to the long pulse lasers with pulse energy at the mJ level, the ultrashort pulse duration of the femtosecond laser allows substantially lower pulsed energies (sub mJ) to be used, which further eliminates the collateral damage.

Recently, ultrashort pulsed lasers have been used in various biomedical applications, including laser tissue manipulation,[1–4] laser surgery,[5–12] and biomedical devices.[13,14] The mechanism and physics of plasma-mediated ablation was studied and reviewed and it was used as a tool to generate targeted insults at the subcellular level to different tissue.[6,9–11] Negligible collateral damage and highly efficient ablation rates have also been demonstrated. High precision subsurface ablation in highly scattering tissues including murine skin and human sclera was studied by using femtosecond laser pulses and multiphoton absorption,[12] demonstrating the ability to target deeper structures in skin using subsurface ablation and to allow novel clinical applications for dermatological laser surgery. However, the advantages of ultrashort pulsed laser surgery have been compromised with the lack of a real-time feedback system to monitor tissue types being ablated and to automatically control laser parameters. This system would be especially useful in the microsurgery for brain and spine, where the risk of damaging peripheral nerves is high and the impact on patients is huge. Although different diagnostics and metrology techniques (e.g., x-ray fluorescence, confocal microscopy, optical coherence tomography (OCT), and fluorescence spectroscopy) have been used to characterize laser material processing,[15,16] these established techniques are slow or impractical for real-time accurate measurements during rapid laser processing of materials.

Laser-induced breakdown spectroscopy (LIBS) is a type of atomic emission spectroscopy that focuses a pulsed laser beam on the target surface to generate plasma. The sample can be in solid, liquid, or gas form. LIBS has the primary advantages of rapid and simultaneous analysis of a wide variety of elements, a small amount of material needed, little or no sample preparation required, and is nondestructive. LIBS has the ability to extract concentrations of the elements based on the intensity level of their corresponding emission lines. Each type of tissue has its own characteristic chemical composition and the concentration of the constituent elements varies from tissue to tissue. Therefore, the emission lines of the same element in different tissues show different intensity ratings on the LIBS spectra. LIBS has been used for real-time process control and quality assurance for industrial applications[17,18] and for laser surgery and biomedical applications.[4,19–30] The laser-induced plasma spectrum can be used to distinguish biological samples based on their chemical composition. In particular, bone and other calcified tissue may be distinguished from soft tissue based on the strong calcium emission peaks.[24] An initial demonstration of feedback controlled surgery involved a perfused and fixed mouse head.[29] Plasma-mediated ablation with ultrashort laser pulses was used to cut an opening in the skull. The laser-induced plasma spectrum was continuously monitored and it was used to shutter the beam when regions of soft tissue were encountered. This procedure led to a precise craniotomy that would be a difficult manual procedure without producing any damage in the sagittal sinus. Performance of femtosecond laser-induced breakdown spectroscopy (fs-LIBS) for the determination of elements in animal tissues was evaluated.[30] Data obtained indicate both that it is a matrix-independent sampling process and that fs-LIBS can be used for the determination of different elements. Given the unique mechanism of the ultrashort pulsed laser, it is well recognized as an ideal candidate for microsurgeries. The integration of this type of laser with real-time LIBS

*Address all correspondence to: Huan Huang, E-mail: hhuang@polaronyx.com

feedback would be essential to ensure precise detection, identification, and control during the rapid laser ablation process. However, simply shutting off the laser when a soft tissue region is detected is insufficient since the detection capability is also turned off and hence the laser surgery itself. No tool or practical device currently exists that combines the cutting using ultrashort laser pulses with negligible collateral tissue damage with real-time feedback control of the cutting process.

In this study, an LIBS-guided smart surgical tool using a 0.5 mJ high energy femtosecond fiber laser is developed. This system features real-time feedback and control of the processing parameters (pulse energy, repetition rate, and speed) to ablate different types of materials including tissues and metals. An automation algorithm is developed to detect and identify materials from LIBS signals and to adjust the laser parameters accordingly. Experiments were successfully carried out to verify the automation algorithm and process.

## 2 Experiment

Figure 1 shows the sketch of the LIBS-guided laser processing system. The major hardware components are a commercial 0.5 mJ high energy mode-locked femtosecond fiber laser system (Uranus-mJ Series, PolarOnyx Laser, Inc.), a microscope objective lens, a three-dimensional (3-D) controllable motion stage (Aerotech, Inc.) on which the sample is mounted, LIBS signal collecting fiber and optics, a fiber-based spectrometer, focusing optics, an acousto-optic modulator (AOM) for laser parameter control, and a computer for data analysis and process control. The laser system generates linearly polarized pulses at 1030-nm wavelength with a 750-fs pulse duration (full width at half maximum) and pulse repetition rate tunable from 1 Hz up to 1 MHz. The output collimated beam is a nearly symmetric Gaussian with $M^2 < 1.3$ and the maximum output pulse energy is 0.5 mJ. Two types of micromachining schemes were used– a microscope objective lens with motion stage and a two-dimensional (2-D) scanner (Scanlab AG) (not shown in Fig. 1) with F-theta lens.

The optical emission from the ablation is collected by a collimator lens and then coupled into a multimode optical fiber and delivered to a spectrometer. The collection optics is oriented with an angle above the processing location. All the experiments are conducted in ambient air. A scientific-grade spectrometer

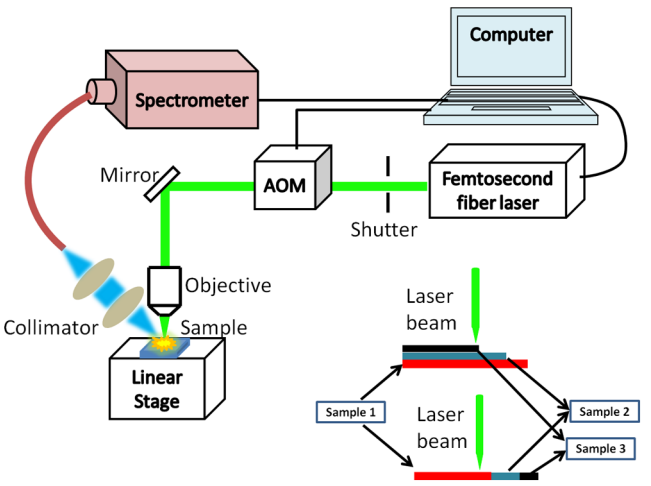


**Fig. 1** Sketch of laser-induced breakdown spectroscopy (LIBS) guided laser processing system.

(QE65000, Ocean Optics, Inc.) with a highly sensitive detector was used. The spectral range of the spectrometer is from ultraviolet to near-infrared (200 to 950 nm). A filter was used during the experiment to block the laser wavelength.

The control system includes machine vision, motion control, LIBS signal processing, laser control, and process control. The machine vision provides the laser micromachining process with a clear camera image on a microscopic scale. The motion control system consists of 3-D linear servomotor stages that adjust the laser beam to focus on moving samples. A 2-D scanner is also integrated in the system. The laser control system adjusts the pulse energy and repetition rate by controlling the AOM analog input and digital input, respectively. The process control uses the automation algorithm to do real-time feedback and process parameter control with different patterns, laser parameters, and focusing conditions.

The sample holder is adjustable to fit different materials. They can be laid out to form a one-layer structure or stacked to form a multilayer structure, as shown in Fig. 1. Optical spectral signals are collected when the laser beam irradiates onto different materials to excite plasma. The spectrum analysis identifies primary chemical elements of the ablated material and then feeds back to the system control.

Fresh tissues (bovine bone, skin, tendon, liver, and muscle) from a local supermarket were used in this study. The tissue samples were carefully washed with sterile saline solution. To better demonstrate the processing control, metals such as aluminum and copper were also used as foreign materials in the test. All measurements were performed in an open environment.

After the laser processing, microtopography of the processed features was characterized and evaluated with an upright digital microscope (ME520T) and a scanning electron microscopy (SEM, FEI QUANTA FEG 600).

## 3 Results

### 3.1 *Laser-Induced Breakdown Spectroscopy Guided System Control and Algorithm*

Figure 2 shows the flow diagram of the LIBS-guided system control with real-time feedback. The target material is ablated with a focused laser beam and a plume of plasma is generated. The optical emission spectrum is collected and analyzed to identify the chemical composition. The analyzed data are then feed back to the laser ablation processing and adjustments are made accordingly.

To reduce the effect of continuum emission and background noise, the LIBS spectra are averaged and normalized. A detection limit is set such that any intensity below the limit is considered as noise or processing not started. The control algorithms can be divided into several categories, including atomic line-matching method, which searches and compares the emission spikes with the atomic emission database. One straightforward and easy approach is to use the typical largest peaks method. The sample spectrum is compared with each of the reference material spectra on the basis of the differences of the intensities at preselected specific wavelengths. A National Institute of Standards and Technology (NIST) reference database is preloaded to the algorithm for identification of the peaks. At least three major characteristic peaks were used for material detection.

To further characterize the material, the relative ratio of peak heights is analyzed. This is especially useful to distinguish

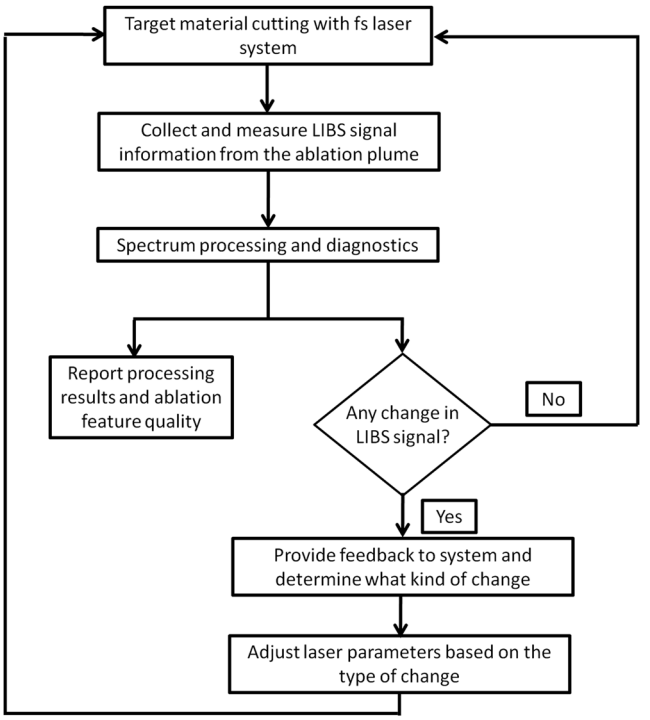


**Fig. 2** Flow diagram for LIBS-guided system control with real-time feedback.

different types of tissues with similar major element compositions, as the concentrations of characteristic elements vary. As an example, the characteristic peaks for bovine bone and skin are very similar, they both have Ca (393.36 nm), Na (588.98 nm), and H (656.56 nm) elements. However, the ratio of the characteristic peaks is different. In bovine bone, Ca has the highest intensity, and Na and H are close to each other. In bovine skin, Na has the highest intensity, and the Ca and H peaks intensities are relatively lower.

The algorithms discussed above were implemented in a real-time computer-controlled system. The program collects sample spectra continuously from the spectrometer during laser ablation and compares them to reference spectra in a database. The program drives a transistor–transistor logic (TTL) signal to control the laser pulse on-off and an analog signal to control the pulse energy of the femtosecond laser via AOM, and drives another digital signal to control the pulse repetition rate of the femtosecond laser. Two factors have to be considered for real-time feedback and detection especially for surgical applications: spectrum acquisition time and the signal processing time.

### 3.2 *Laser-Induced Breakdown Spectroscopy for Material and Tissue Identification*

To be an efficient real-time feedback tool, the LIBS signal should be sensitive only to the ablated material's elemental composition, and insensitive to other factors, such as laser parameters and the interaction environment.

Figure 3 shows an example of an LIBS spectrum for metal and glass materials taken by the femtosecond fiber laser system. The pulse energy is 0.75 $\mu$J and repetition rate is 225 kHz. The atomic emission peaks in Fig. 3(a) are aluminum at wavelengths of 309.28 and 396.16 nm. The atomic emission peaks in Fig. 3(b) are Ca (393.36 and 396.85 nm), Mg (517.27 and 518.36 nm), Na (588.98 nm), and K (766.49 and 769.90 nm), respectively. As shown in Fig. 3, the plasma emission continuum is minimal, in contrast to what is commonly observed with a ns laser with higher pulse energies. As shown in previous studies,[15,20,21] femtosecond laser-based LIBS signal is insensitive to laser parameters (e.g., laser fluences) and the spatial configuration of the spectrometer detector (e.g., detector angle from the laser incident direction).

Figure 4 shows an example of an LIBS spectrum for different tissues using the 0.5 mJ femtosecond fiber laser system. The atomic emission peaks of bovine bone in Fig. 4(a) include Ca (393.36 and 396.85 nm), Mg (517.27 and 518.36 nm), Na (588.98 nm), H (656.56 nm) and K (766.49 and 769.90 nm), respectively. In comparison, major atomic emission peaks are also seen in the LIBS spectra of other bovine tissue types in Fig. 4(b). The main elemental compositions are similar, but the intensities levels and ratios of LIBS spectra vary. This information is useful for differentiating various tissue types.

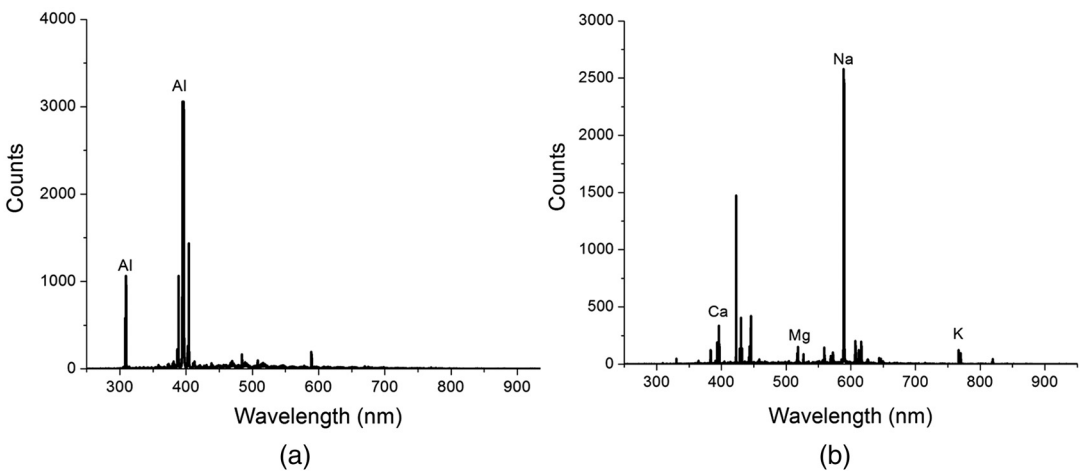


**Fig. 3** Measured LIBS signal using femtosecond fiber laser processing system: (a) aluminum; (b) soda lime glass.

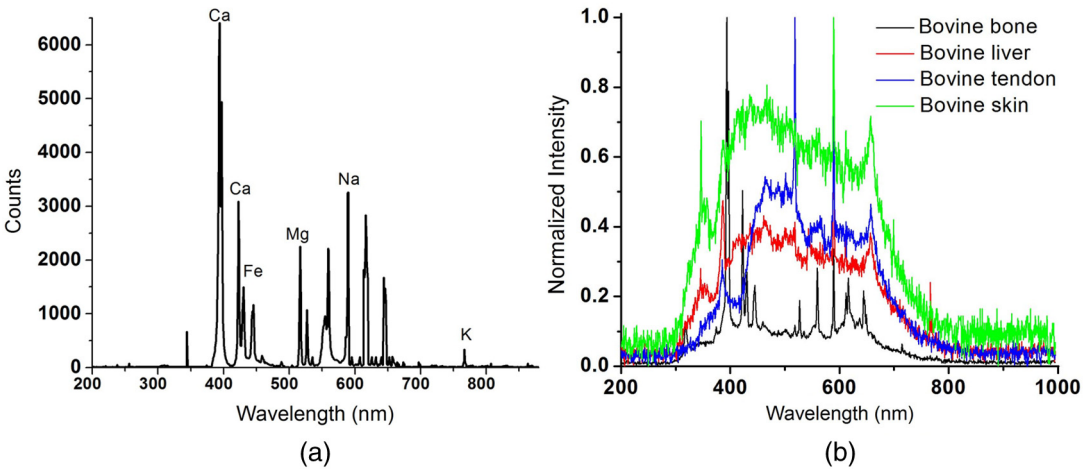


**Fig. 4** Measured LIBS signal using femtosecond fiber laser processing system: (a) bovine bone; (b) comparison of different types of bovine tissues.

### 3.3 *Smart Surgical Tool Implementation and Verification*

The real-time control system was implemented to process different tissue samples (bovine bone and skin). Two metals (aluminum and copper) were also added to test the system's sensitivity and selectivity. During the process, the laser beam scans from one sample to another. Table 1 shows the major elements monitored in the experiments for different materials.

To verify the system performance, the samples undergo cutting by laser beam without LIBS control. The process parameters remain unchanged when the beam hits various samples. As soon as the LIBS feedback control is enabled, the stage moving speed, pulse energy, and repetition rate are adjusted based on the material type and preoptimized laser processing conditions for each material. The time to switch between processing programs is estimated to be a few tens of milliseconds. Figure 5(a) shows the material samples used in this experiment. Figures 5(b) to 5(e) show the screen shots of different material detections with the indicators and the transitions from aluminum, copper, bovine bone to bovine skin with the LIBS spectrum are clearly observed. Compared with laser processing without any feedback control, the controlled ablation approach provides several major advantages including less material damage and higher precision with on demand laser processing conditions. Figure 5(f) shows an overview of the laser processing test with real-time feedback and the ablation spark and LIBS signal can be seen from the monitor. The experimental set-up is also partially shown in Fig. 5(f).

**Table 1** Major elements monitored in the experiments for different materials.

| Element type (nm) | Bovine bone | Bovine skin | Aluminum | Copper |
|---|---|---|---|---|
| Na-588.98 | x | x | — | — |
| Ca-317.90, 393.36,396.85 | x | x | — | — |
| N-862.92 | x | x | — | — |
| O-777.32 | x | x | — | — |
| H-656.56 | x | x | — | — |
| Al-309.28, 396.16 | — | — | x | — |
| Cu-324.75, 327.39, 510.55, 515.32,521.82 | — | — | — | x |

The real-time feedback and control laser processing system is used to demonstrate tissue cutting and drilling applications. Figure 6 shows the SEM overview of the hole drilling results in bovine bone. The laser parameters include 25 $\mu$J pulse energy, 50 kHz repetition rate, and 1 mm/s drilling speed. The depth of bovine bone is about 300 $\mu$m. The drilled hole has an entrance diameter of 230 $\mu$m and an exit diameter of 173 $\mu$m. The drilled holes have good circular geometry for both entrance and exit sides and no thermal damage is observed around the edges. The laser parameters were kept constant and the LIBS feedback can inform when the hole drilling starts and when the hole is drilled through.

Furthermore, trench micromachining and cutting were also studied. Figure 7 gives an example of bovine bone trench micromachining using a femtosecond fiber laser. The trench width is 400 $\mu$m and depth is about 760 $\mu$m. The laser parameters are 100-kHz repetition rate and 25-$\mu$J pulse energy. The scanning speed is 200 mm/s and multiple lines were used in the trench writing. From the cross-section view, it is observed that side walls are almost vertical and the angles on both sides are around 85 deg near the opening of the trench; when the trench goes deeper, the side wall angles decrease and the trench becomes a "U" shape. Figure 7(b) shows a detailed SEM view of the side wall. The trench wall is straight and clean without any thermal damage.

As shown in Figs. 6 and 7, it is remarkable to find no visible cracks or thermal damage around the edges of the drilled holes, which is differentiated from CW and long pulsed (ns to ms pulse width) lasers. Typically, treatment by those conventional lasers leads to cracking, melting, and charring of the surrounding materials from a few tens of microns to a few hundreds of microns range.[31,32]

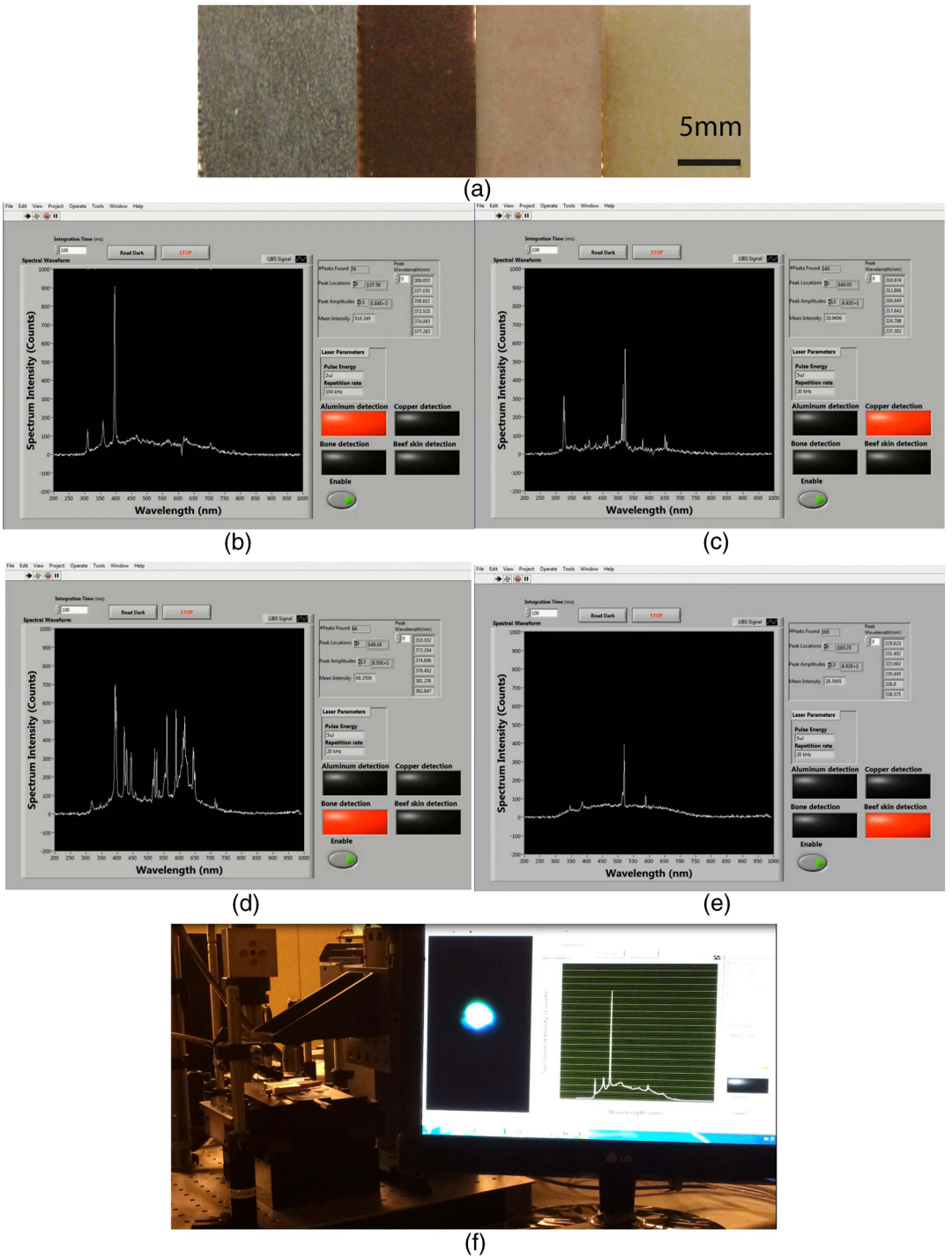


**Fig. 5** (a) Photograph of materials samples used in the experiment, from left to right–aluminum, copper, bovine bone and bovine skin; (b)-(e) screen shots of different material detections with the red indicator to show the transitions from (b) aluminum, (c) copper, (d) bovine bone to (e) bovine skin; (f) overview of real-time feedback and control of laser processing-ablation plasma image, spectrum and material indicator for aluminum detection.

Figure 8 shows another example of bovine tissue cutting and drilling using femtosecond laser processing with real-time feedback. The laser parameters used are 100-kHz repetition rate and 15-$\mu$J pulse energy. Figure 8(a) shows the cutting of bovine muscle with a 100-$\mu$m cutting width and the total thickness is 200 $\mu$m. Figure 8(b) shows the drilling of bovine muscle with a 300-$\mu$m hole diameter and the thickness is 400 $\mu$m. No visible cracks or thermal damage is evident around the edges of the drilled hole. It is important to note the LIBS signals were analyzed during the cutting and drilling process to identify where the tissue boundary is and decide when the process starts and ends. Depending on the material type and processing status, the feedback system could then decide whether to continue or stop the exposure. Such an integrated system prevents the damage of other types of materials or tissue during complex laser surgery.

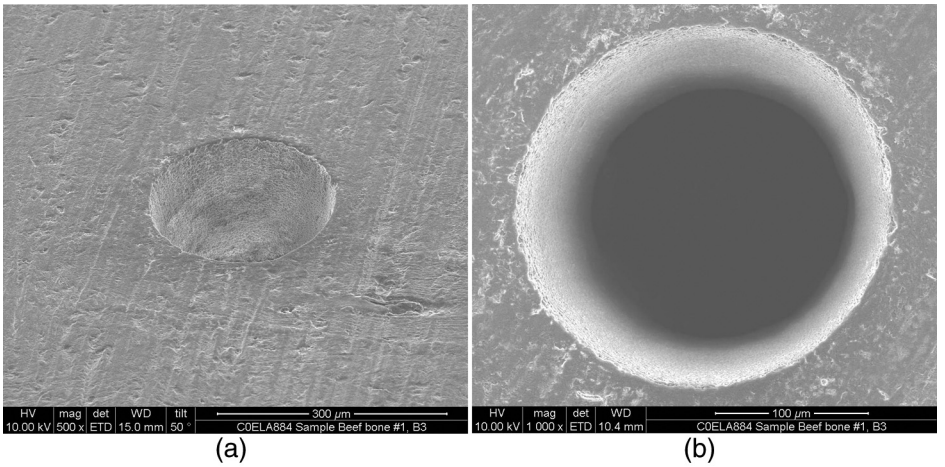


**Fig. 6** Scanning electron microscopy (SEM) view of microhole drilling in bovine bone by using LIBS-guided smart surgical tool: (a) overview; (b) top view.

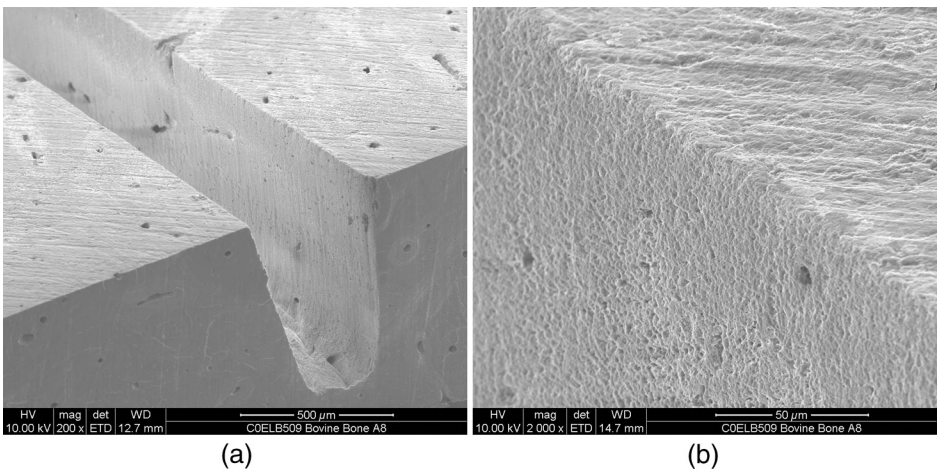


**Fig. 7** (a) SEM cross section view of trench in bovine bone written by using LIBS-guided smart surgical tool; (b) SEM detailed view of the side wall.

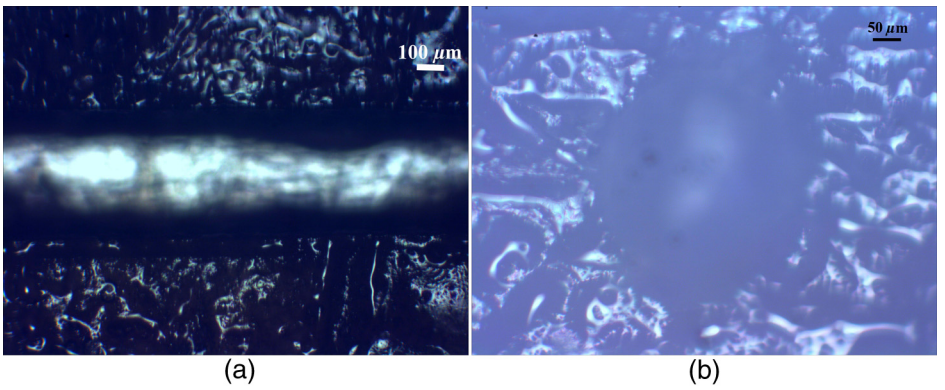


**Fig. 8** (a) Bovine muscle cutting by using LIBS-guided smart surgical tool; (b) bovine muscle drilling by using LIBS-guided smart surgical tool.

## 4 Summary and Conclusion

A LIBS-guided smart surgical tool using a femtosecond fiber laser is developed and demonstrated. This functional system successfully demonstrated automatic material ablating capability with: (1) real-time detection and identification of ablated materials; (2) real-time adjustment of process parameters including pulse energy, repetition rate, and scanning speed; (3) automatic contour pattern for any shape or size for different applications such as drilling and cutting; and (4) free of cracks and thermal damage. This study provides a powerful

LIBS-guided smart surgical tool for precise robotic microsurgery procedures.

Future works will focus on *in situ* and *in vivo* tissue ablation in animal models and further integration of the system into an all fiber-based portable version for clinic applications.

## Acknowledgments

This work was partially funded by Department of Energy and Army Small Business Innovation Research programs.

## References

1. N. Shen et al., "Photodisruption in biological tissues and single cells using femtosecond laser pulses," presented at *Conf. on Lasers and Electro-Optics, (CLEO 2001)*, Technical Digest, pp. 403–404, IEEE, Baltimore, Maryland (2001).
2. H. Huang and Z. Guo, "Human dermis separation via ultra-short pulsed laser plasma-mediated ablation," *J. Phys. D* **42**, 165204 (2009).
3. Y. Liu and M. Niemz, "Ablation of femural bone with femtosecond laser pulses-a feasibility study," *Laser Med. Sci.* **22**, 171–174 (2007).
4. A. Rode et al., "Precision ablation of dental enamel using a subpicosecond pulsed laser," *Aust. Dent. J.* **48**(4), 233–239 (2003).
5. M. Strassl et al., "Ultra-short pulse laser ablation of biological hard tissue and biocompatibles," *J. Laser Micro/Nanoeng.* **3**, 30–40 (2008).
6. A. Vogel et al., "Mechanisms of femtosecond laser nanosurgery of cells and tissues," *Appl. Phys. B* **81**, 1015–1047 (2005).
7. W. Watanabe et al., "Femtosecond laser disruption of subcellular organelles in a living cell," *Opt. Express* **12**, 4203–4213 (2004).
8. L. T. Nordan et al., "Femtosecond laser flap creation for laser in situ keratomileusis: six-month follow-up of initial US clinical series," *J. Refract. Surg.* **19**(1), 8–14 (2002).
9. P. S. Tsai et al., "Plasma-mediated ablation: an optical tool for submicrometer surgery on neuronal and vascular systems," *Curr. Opin. Biotech.* **20**(1), 90–99 (2009).
10. J. Qiu et al., "Femtosecond laser lithotripsy: feasibility and ablation mechanism," *J. Biomed. Opt.* **15**(2), 028001 (2010).
11. J. Neev et al., "Surgical and dental applications of ultrashort pulse lasers," *IEEE Lasers Electro-Opt. Soc. Ann. Meet.*, Vol. 1, pp. 261–262 (1996).
12. J. Qiu et al., "Deep subsurface cavities in skin utilizing mechanical optical clearing and femtosecond laser ablation," *Lasers Surg. Med.* **45**, 383–390 (2013).
13. S. D. Gittard and R. J. Narayan, "Laser direct writing of micro-and nano-scale medical devices," *Expert Rev. Med. Devices* **7**(3), 343–356 (2010).
14. C. L. Hoy et al., "Clinical ultrafast laser surgery: recent advances and future directions," *IEEE J. Sel. Topics Quantum Electron.* **20**, 1–14 (2014).
15. F. Stelzle et al., "The impact of laser ablation on optical soft tissue differentiation for tissue specific laser surgery-an experimental *ex vivo* study," *J. Transl. Med.* **10**, 123 (2012).
16. S. A. Boppart et al., "High-resolution optical coherence tomography-guided laser ablation of surgical tissue," *J. Surg. Res.* **82**, 275–284 (1999).
17. J. Eberhard et al., "Evaluation of selective caries removal by a fluorescence feedback-controlled Er: YAG laser *in vitro*," *Caries Res.* **39**(6), 496–504 (2005).
18. R. Noll et al., "Laser-induced breakdown spectrometry-applications for production control and quality assurance in the steel industry," *Spectrochim. Acta B* **56**, 637–649 (2001).
19. T. Tong, J. Li, and J. P. Longtin, "Real-time control of ultrafast laser micromachining by laser-induced breakdown spectroscopy," *Appl. Opt.* **43**, 1971–1980 (2004).
20. M. L. DeVeaux, "Evaluation of statistical methods for classification of laser-induced breakdown spectroscopy (LIBS) data," PhD Thesis, Mount Holyoke College (2012).
21. H. Imam, R. Mohamed, and A. A. Eldakrouri, "Primary study of the use of laser-induced plasma spectroscopy for the diagnosis of breast cancer," *Opt. Photonics J.* **2**, 193 (2012).
22. D. C. Jeong, P. S. Tsai, and D. Kleinfeld, "Prospect for feedback guided surgery with ultra-short pulsed laser light," *Curr. Opin. Neurobiol.* **22**, 24–33 (2012).
23. R. Kanawade et al., "Pilot study of laser induced breakdown spectroscopy for tissue differentiation by monitoring the plume created during laser surgery: an approach on a feedback laser control mechanism," *Spectrochim. Acta B* **87**, 175–181 (2013).
24. H. Huang, L.-M. Yang, and J. Liu, "Qualitative assessment of laser-induced breakdown spectra generated with a femtosecond fiber laser," *Appl. Opt.* **51**, 8669–8676 (2012).
25. O. Samek, H. H. Telle, and D. C. Beddows, "Laser-induced breakdown spectroscopy: a tool for real-time, *in vitro* and *in vivo* identification of carious teeth," *BMC Oral Health* **1**, 1 (2001).
26. A. Kumar et al., "Characterization of malignant tissue cells by laser-induced breakdown spectroscopy," *Appl. Opt.* **43**, 5399–5403 (2004).
27. M. Baudelet et al., "Discrimination of microbiological samples using femtosecond laser-induced breakdown spectroscopy," *Appl. Phys. Lett.* **89**, 163903 (2006).
28. B.-M. Kim et al., "Optical feedback signal for ultrashort laser pulse ablation of tissue," *Appl. Surf. Sci.* **127**, 857–862 (1998).
29. D. Jeong et al., "All optical cranial surgery: ablation of hard but not soft tissue by amplified femtosecond laser pulses and feedback from atomic emission spectra," in *Proc. Society for Neuroscience Annual Meeting*, Society for Neuroscience, San Diego (2010).
30. D. Santos et al., "Evaluation of femtosecond laser-induced breakdown spectroscopy for analysis of animal tissues," *Appl. Spectrosc.* **62**(10), 1137–1143 (2008).
31. K. M. Sasaki et al., "Ultrastructural analysis of bone tissue irradiated by Er: YAG laser," *Laser Surg. Med.* **31**, 322–332 (2002).
32. T. J. Flotte, R. Anderson, and T. F. Deutsch, "Pulsed CO2 laser tissue ablation: effect of tissue type and pulse duration on thermal damage," *Laser Surg. Med.* **8**, 108–118 (1988).

**Huan Huang** is now a project manager in PolarOnyx, Inc. He received his BS and MS in mechanical engineering from Tsinghua University in 2003 and 2005, and his PhD in mechanical engineering from Rutgers University in 2010. His research interests include laser material interaction physics, laser 3D printing/additive manufacturing, laser tissue interactions, laser micro/nanofabrication, laser-induced breakdown spectroscopy and novel laser-processing technology development.

Biographies of the other authors are not available.